Molecular Basis of Enrofloxacin Translocation through OmpF, an Outer Membrane Channel of *Escherichia coli* - When Binding Does Not Imply Translocation

Kozhinjampara R. Mahendran,[†] Eric Hajjar,[‡] Tivadar Mach,[§] Marcos Lovelle,[§] Amit Kumar,[‡] Isabel Sousa,[§] Enrico Spiga,[‡] Helge Weingart,[†] Paula Gameiro,[§] Mathias Winterhalter,[†] and Matteo Ceccarelli*[,‡]

Jacobs University Bremen, Campus Ring 1, D-28759 Bremen, Germany, Istituto Officina dei Materiali CNR, UOS Slacs and Dipartimento di Fisica, Universita di Cagliari, S.P. Monserrato Sestu Km 0.700, I-09042 Monserrato (CA), Italy, and Requimte, Faculdade de Ciencias, Universidade do Porto, Rua do Campo Alegre, 4169-007 Porto, Portugal

Received: December 3, 2009; Revised Manuscript Received: January 25, 2010

The molecular pathway of enrofloxacin, a fluoroquinolone antibiotic, through the outer membrane channel OmpF of *Escherichia coli* is investigated. High-resolution ion current fluctuation analysis reveals a strong affinity for enrofloxacin to OmpF, the highest value ever recorded for an antibiotic-channel interaction. A single point mutation in the constriction zone of OmpF, replacing aspartic acid at the 113 position with asparagine (D113N), lowers the affinity to a level comparable to other antibiotics. All-atom molecular dynamics simulations allow rationalizing the translocation pathways: wild-type OmpF has two symmetric binding sites for enrofloxacin located at each channel entry separated by a large energy barrier in the center, which inhibits antibiotic translocation. In this particular case, our simulations suggest that the ion current blockages are caused by molecules occupying either one of these peripheral binding sites. Removal of the negative charge on position 113 removes the central barrier and shifts the two peripheral binding sites to a unique central site, which facilitates translocation. Fluorescence steady-state measurements agree with the different location of binding sites for wild-type OmpF and the mutant. Our results demonstrate how a single-point mutation of the porin, and the resulting intrachannel shift of the affinity site, may substantially modify translocation.

Introduction

To reach their target in Gram-negative bacteria, antibiotic molecules must first permeate through the outer membrane, a complex macromolecular assembly comprising a hydrophobic lipid bilayer with pore-forming proteins.[1] The selectivity of this membrane barrier has a major impact on antibiotic translocation and consequently on their efficiency.[2] In *Escherichia coli,* OmpF is considered a major pathway for the translocation of the newer generations of beta-lactam and quinolone antibiotics.[3] The OmpF high-resolution X-ray structure reveals a homotrimer, with each monomer forming a separate β-barrel composed of sixteen β-strands spanning the outer membrane.[4] A key feature in the structure of OmpF shown in Figure 1A is the presence of a constriction region (CR) due to the loop L3, which folds back into the channel, forming both a steric and electrostatic hindrance. This zone is characterized by a strong transversal electric field, generated by the negatively charged residues D113 and E117 (L3 side) facing a cluster of positively charged residues R42, R82, and R132 (anti-L3 side). While OmpF is a general diffusion porin, not showing affinity-enhanced uptake like substrate-specific channels in its normal function,[5] antibiotics can exploit naturally present residues to find a weak binding site, thereby increasing their influx.[6]

Fluoroquinolones are among the most commonly used classes of antibiotics in human and veterinary medicine.[7] While quinolones' mechanism of action is based on inhibiting the catalytic activity of two enzymes essential to the replication of bacterial DNA (DNA gyrase and Topoisomerase IV),[8] their activity can be strongly affected by their accumulation in bacteria.[9,10] The two possible pathways for antibiotic influx through the outer membrane are lipid-mediated and general diffusion porins-mediated.[11] Although earlier hydrophobic quinolones can diffuse across the outer lipid membrane, it has been suggested that several newer more effective hydrophilic quinolones[12] use OmpF to gain access to the cell interior, with resistant strains showing specifically loss of the OmpF porin.[13,14] Changes in antibiotic influx are also seen upon point mutations in OmpF,[15–17] and several resistant strains have porins with a sequence modified as compared to their susceptible counterparts.[18] Previous biological and docking studies implicated D113 as an important residue for antibiotic binding and uptake,[19] however, the molecular mechanisms of any such process are poorly understood.

Using single-channel conductance measurements through reconstituted wild-type (WT) OmpF, we find an unexpectedly strong affinity of enrofloxacin, a zwitterionic second-generation fluoroquinolone. This affinity is comparable to substrate interaction with specific channels (e.g., maltose with maltoporin[20]) and led us to select enrofloxacin as a model system for further study. Interestingly, we find that the strong affinity decreases drastically upon a single point mutation - replacing the aspartic acid at the 113 position with asparagine (D113N) lowers the binding strength to one comparable to other antibiotics. Although the hydrophobicity of enrofloxacin is very high,[21] its structure (Figure 1B) only slightly differs from that of fluoroquinolones known to efficiently cross the outer membrane through OmpF analogues, while displaying weaker binding than enrofloxacin;

* To whom correspondence should be addressed.
[†] Jacobs University Bremen.
[‡] Università di Cagliari.
[§] Universidade do Porto.

10.1021/jp911485k © 2010 American Chemical Society
Published on Web 03/29/2010

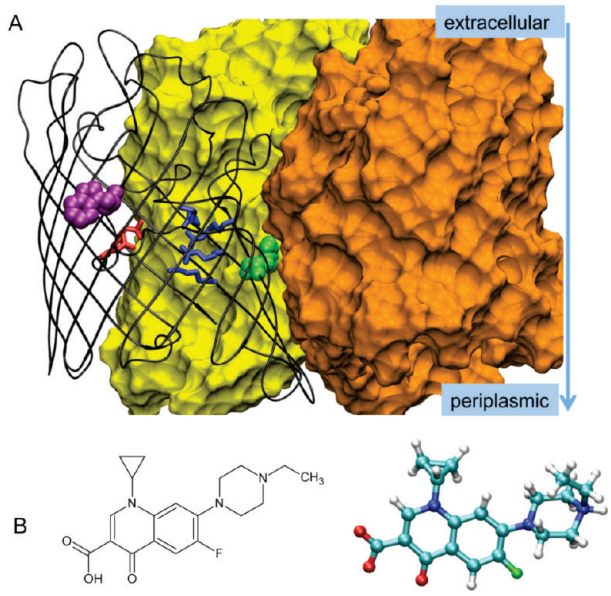

Figure 1. (A) 3D structure of the OmpF homotrimer. The first monomer is displayed in cartoons to highlight its secondary structures, while the second and third monomers are displayed in a surface representation and colored in yellow and orange, respectively. The two tryptophan residues are represented in van der Waals and colored in green for W61 and purple for W214. The charged residues at the CR are colored by residue type: blue for positively charged, red for negatively charged. (B) Structure of enrofloxacin, and the 3D structure of its optimized geometry, obtained as explained in the Experimental Section. (The molecule is colored by atom types: blue for nitrogen, red for oxygen, cyan for carbon).

a single ethyl group difference compared to ciprofloxacin[22,23] and a different hydrophobic group compared to moxifloxacin.[24] It becomes interesting to see whether the stronger interaction translates to increased translocation, as in the case of substrate-specific channels, and how small structural changes in the constriction zone have a strong effect.

Using high-resolution ion current analysis, fluorescence spectroscopy, and atomistic computer simulations in conjunction with a single site mutation, we arrive at a consistent picture of the enrofloxacin interaction and translocation through the OmpF porin. We show that by combining different techniques one obtains information on the molecular mechanism of transport. Drawing general conclusions from this model system allows us to elucidate important details of substrate-channel interactions, which is of interest for rational antibacterial design and screening.

Experimental Section

All chemicals used were from Merck (Darmstadt, Germany) (pro analysi), except KCl, KOH, HCl and *N*-(2-hydroxyethyl)piperazine-*N*-ethanesulfonic acid (HEPES) (Applichem, Darmstadt, Germany), *n*-octylpolyoxyethylene (octyl-POE) (Bachem, Bubendorf, Switzerland), chloroform, hexadecane, and hexane (Fluka, Buchs, Switzerland) and all lipids from Avanti Polar Lipids (Alabaster, AL). Doubly distilled and deionized water was used to prepare all solutions. Enrofloxacin was obtained from Fluka (Buchs, Switzerland).

The site-directed mutagenesis using origin repair to obtain the D113N expression plasmid, and the purification of OmpF from *E. coli*, strain BL21 (DE3) Omp8d, was done following published procedures.[25,26]

Conductance Measurements. The enrofloxacin stock solution for conductance measurements was made at a final concentration of 2.0 mM in 150 mM KCl, 10 mM 2-(*N*-morpholino)ethanesulfonic acid (MES) (pH 5.5). Planar lipid bilayers were formed with the monolayer opposition technique[27] across a 40 μm diameter circular aperture in a 25 μm thick polytetrafluoroethylene film (Goodfellow, Cambridge, U.K.) being tightly glued between two Delrin chambers manufactured in-house, each containing 200 μL of an aqueous bathing solution, through the layering of 1 μL of a 5 mg/mL solution of 1,2-diphytanoyl-*sn*-glycero-3-phosphatidylcholine (DPhPC) dissolved in pentane on the buffer surface on each side. One to two microliter OmpF porin micellar suspensions from a 1.5 ng/mL solution in 150 mM KCl with 1% octyl-POE was added to the cis side compartment (contacted by the ground electrode). Incorporation was achieved by stirring after addition and applying a 200 mV transmembrane voltage.

OmpF inserts into artificial bilayers in a strictly ordered manner: there is a strong indication that the porin inserts with periplasmic loop first, that is, if the protein is added to the cis side, the normally periplasmic side is on the trans side and the extracellular side is on the cis side.[28,29] Electrical recordings were made through a pair of Ag/AgCl electrodes (World Precision Instruments, Sarasota, FL), attached to an Axon Instruments 200B amplifier with a capacitive headstage, digitized by an Axon Digidata 1322A digitizer, computer controlled by Clampex 10.0 software (all by Axon Instruments, Foster City, CA). The data was filtered by an analogue low-pass four-pole Bessel filter at 10 kHz, and digitally sampled at 50 kHz. Data analysis was carried out on the Clampfit 10.0 software (Axon Instruments). The concentration of antibiotic was adjusted by solution exchange in the appropriate compartments, not changing the total aqueous volume. At every addition stage the concentration was corroborated by subsequent UV−visible (UV−vis) absorption from liquid samples withdrawn after measurement.

Fluorescence Studies. OmpF concentration was estimated using the bicinchoninic acid protein assay against bovine serum albumin as the standard.[30,31] All solutions for fluorescence measurements were prepared with 10 mM HEPES buffer (0.1 M NaCl; pH 7.4). Spectrophotometric and fluorescence measurements were performed in a Varian spectrofluorometer, model Cary Eclipse and a UNICAM UV-300 spectrophotometer, both equipped with a constant-temperature cell holder (Peltier single cell holder). All of the spectra were recorded at 37 °C, under constant stirring, with a slit width of excitation and emission of 10 nm, from 305 to 400 nm for emission and 290 nm for excitation. Inner filter effects and dilution of the solution were accounted for.

OmpF proteoliposomes were prepared by direct incorporation into preformed liposomes of 1,2-dimyristoyl-*sn*-glycero-3-phosphocholine (DMPC) by well-established methodology,[32–34] using a 100 nm diameter extruded liposome suspension (2 mM lipid concentration) and detergent-solubilized OmpF (1 mg/mL protein in 1% octyl-POE) to achieve a final protein−lipid molar ratio of 1:1000. The proteoliposomes were extruded after formation through a 600 and subsequently a 100 nm polycarbonate membrane (Whatman, Maidstone, UK) to guarantee the homogeneity of the size distribution in the suspension.

Enrofloxacin fluorescence quenching studies were achieved by successive additions of a constant volume (10 μL) of enrofloxacin solution to the cuvette (final concentration range: 0−7.5 μM) containing a constant amount of OmpF (0.45 μM) incorporated in liposomes. The acrylamide and iodide fluorescence quenching studies were achieved by successive additions of a constant volume (10 μL) of acrylamide or KI solutions (5.0 M) to the cuvette (final concentration range: 0.0−0.5 M)

containing a constant amount of OmpF (0.45 μM) inserted in liposomes, in the absence or in the presence of a certain constant quantity (final concentration 7.4 μM) of enrofloxacin. The first UV−vis and fluorescence spectrum was taken before the additions (with only protein suspension or protein suspension plus constant amount of quinolone), and then after each addition the fluorescence spectrum and absorption at the excitation wavelength (290 nm) were obtained. Equation fitting was performed using Origin 7.0 software (OriginLab, Northampton, MA).

Starting Structures for Molecular Dynamics (MD) Simulations. The starting structure for the WT OmpF was prepared as described earlier.[35] Briefly, we used one monomer of the crystal structure "2OMF" (PDB code) at a resolution of 2.4 Å. The hydrogens, missing in the X-ray structure, were added using the program ORAC.[36] The residues were protonated as in the work of Im et al., 2002,[37] and we added the required amount of Cl^- and K^+ counterions to neutralize the protein charges. We embedded the system in a hydrophobic environment of detergent molecules (lauryl dimethyl amine oxide, LDAO) and solvated the system with ~8000 water molecules in an hexagonal box. We used the Amber 95 force field and TIP3P model for water.[38] The force field for the enrofloxacin antibiotic was derived following the Amber force field rules with respective charges obtained from the Gaussian program (6-31G** basis set) on the optimized geometry of the molecule. The porin mutant was obtained by molecular replacement using the program ORAC. All simulated systems were validated for convergence and stabilization of energy, temperature, and root-mean-square deviation with respect to the starting structure. Our choice of using OmpF as a monomer is justified by previous studies that reported mutual independence of the three monomers (no cooperativity) for ion, small molecule transport, and antibiotics.[6,39,40]

Metadynamics Algorithm. The antibiotic translocation could be simulated thanks to the incorporation of a novel simulation algorithm, metadynamics, which allows investigating rare events.[41] Briefly, this algorithm employs a bias to accelerate the evolution of some collective variables, defined as the relevant reaction coordinates for the process under investigation, in this case the translocation of enrofloxacin through OmpF. The bias consists of a history-dependent potential, which is constructed as the sum of the repulsive potential centered along the trajectory of the collective variables. These additional energy terms avoid revisiting the same conformations or at least add a penalty term to the previously visited conformations. On the basis of previous findings,[42,35] we have chosen two relevant collective variables: (i) the z-axis or axis of diffusion, defined as the difference between the center of mass of the antibiotic and the center of mass of the system (porin+detergent) along the z-axis; and (ii) the angle θ, which defines the orientation of the long axis of the molecule with respect to the z-axis. A Gaussian potential is added every 4 ps with a height of 1.0 kJ/mol and width of 0.4 Å and 5.0°, respectively, for the distance Z and the angle. These parameters were chosen to allow a better resolution in the sampling of the free energy surface (FES), and we estimate the total error of our simulation strategy to be around 2 kcal/mol. Using such biased simulation strategy, we obtained translocation of enrofloxacin through WT OmpF and D113N after 36 and 27 ns, respectively.

The metadynamics algorithm allows the reconstruction of the free energy in the subspace of the collective variables by integrating the history-dependent terms. Due to the complexity of the process studied, we calculated the free energy after obtaining the first and only translocation path. This first crossing is considered to be the most probable path because it passes through the lowest saddle point. This procedure has been used in many studies, for example Laio and co-workers studied[43] the unthreading of a molecule from a cage and provided an escape energy in good agreement with experimental results. This approximated FES is used to select the regions of energy minima and further calculate the correct energy barriers for each transition as explained in the following.

Free Energy Profiles and Molecular Simulations Analysis. From each metadynamics simulation, we reconstructed the FES in two dimensions for the translocation process. As we were dealing with rather complex FES, with different minima separated by barriers, we further extracted the structures corresponding to each relevant minimum. Each of these structures were the starting point of equilibrium simulations (lasting 1 ns). In depth analysis using VMD and in-house scripts was performed to characterize the following key structural features:

(i) The atomic root-mean-square fluctuations (rmsf's) were calculated for each heavy atoms of the backbone of the antibiotic with respect to its average position during the MD simulations.

(ii) Existence of Hb's and Hc's between atoms of the antibiotics and of OmpF. Hb's are counted using VMD scripts according to the following threshold parameters: a distance of at most 3 Å and donor−hydrogen−acceptor angle of at least 130°. Hc's are counted when nonpolar atoms are separated by at most 3 Å. We then also report the lifetime (probability of existence along simulation) of each interaction between atoms of the antibiotic and atoms of OmpF.

An additional metadynamics simulation was launched starting from the preferred minimum found along the translocation paths, and this enabled calculating the forward and backward energy barriers. On the basis of these data, we finally reconstructed the one-dimensional (1D) free energy profile for the translocation of enrofloxacin through WT OmpF and the mutant. The profiles only report the energetic barriers from the entrance of the antibiotic in the channel to when it reaches the highest barrier (also called the main, effective barrier). In fact, once the antibiotic crosses the CR, we expect a diffusive regime, with no significant affinity sites. The error bars associated with the energy barrier calculations were assessed as done previously[43] and are of 2 kcal/mol at most.

Cross-sectional solvent accessible surface (SAS) area calculations were done using our in-house program HOPE, which compares well with the widely used HOLE program. The HOPE program uses a three-dimensional grid that covers the surface of the protein with a 0.25 Å grid spacing. The algorithm uses a spherical probe of radius 1.4 Å to search for unoccupied points, which do not overlap with the van der Waals radius of the protein atoms (van der Waals radius parameters were taken from the AMBER force field).[38] Finally, the area is obtained by summing the total number of unoccupied points on planes at different Z, the axis of diffusion.

Results and Discussion

Current Recordings. High-resolution ion conductance measurements through a single OmpF trimer reconstituted into a planar lipid bilayer allowed the quantification of antibiotic-channel interaction.[6] As shown in Figure 2, addition of enrofloxacin to the system causes transient blockages of the ionic current (Figure 2B). Surprisingly, already a relatively low concentration of enrofloxacin concurrently blocks two and

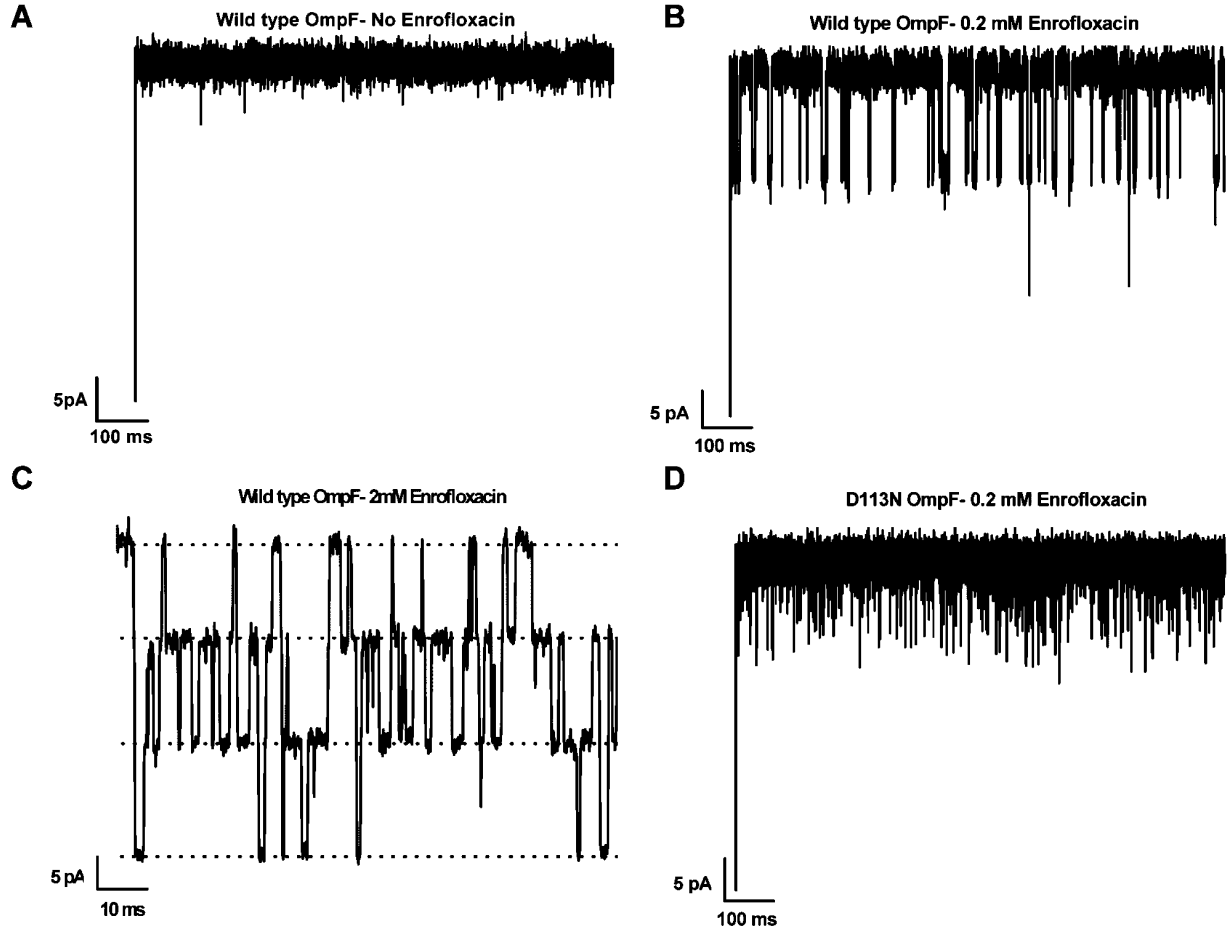

Figure 2. Current absolute values of a single OmpF trimer inserted into a solvent-free planar lipid bilayer, with a potential difference of −50 mV applied (approximately corresponding to the physiological potential[51]), using a 10 kHz low-pass filter in 1 M KCl, 10 mM MES: (A) WT OmpF in the absence of antibiotic, (B) WT OmpF with 200 μM enrofloxacin in the cis chamber, (C) WT OmpF with 2 mM enrofloxacin in the cis chamber, with concurrent blocking of all three monomers visible, and (D) D113N OmpF with 200 μM enrofloxacin in the cis chamber.

eventually all three monomers (Figure 2C), as so far only seen in substrate-specific channels.[44] Figure 3A shows that, in the case of WT OmpF, the number of binding events ν increases linearly with the concentration of the antibiotic and does not significantly depend on the side of antibiotic addition. Residence times were calculated by dwell time analysis[45–47] fitting a single exponential decay to a blocked-time histogram (see Supporting Information). The perfect single-exponential fit indicates an escape over one potential barrier height.[48,49] The average residence time of enrofloxacin was calculated to be 3 ± 0.4 ms at −50 mV and 1.5 ± 0.3 ms at +50 mV. The average residence time τ, while being strongly voltage dependent, does not depend on the concentration or the side of the antibiotic addition (Figure 3B). Kinetic parameters for the asymmetric and symmetric drug addition were calculated using the formulas by Schwarz et al.[50] and are summarized in Table 1. A striking observation is the high value of the calculated binding constant of enrofloxacin in the case of the WT OmpF, $K_{eq} = 96\ M^{-1}$, which is the highest value ever recorded for an antibiotic-channel interaction, comparable to the specific affinity of malto-oligosaccharides to maltoporin.[20]

We mutated aspartic acid at the 113 position to asparagine (D113N) and studied the ion current fluctuations in the presence of enrofloxacin. Enrofloxacin interacts with D113N OmpF resulting in the blockage of ion current in a concentration dependent manner (Figure 2D). The substitution of aspartate by asparagine at the 113 position strongly reduces the equilibrium binding constant between OmpF and enrofloxacin (mainly due to an increased off-rate), which confirms that D113 is an important residue determining the antibiotic−channel interaction. The average residence time of enrofloxacin was calculated to be 100 μs in D113N OmpF irrespective of the sign of applied voltage. The loss of the marked voltage asymmetry shows that in the case of WT OmpF, aspartic acid at 113 might play an important role in the voltage asymmetry of the enrofloxacin interaction.

In the case of D113N OmpF, the number of events is strongly dependent on the side of drug addition, more in line with the asymmetry of OmpF toward the CR.[4] When the antibiotic is added to the cis (extracellular) side of the chamber, the binding events are about twice as frequent as those on the trans (periplasmic) side addition (Figure 3A). The kinetic analysis of ion current blockages through D113N OmpF revealed an on- and off-rate that is substantially increased compared to WT OmpF.

The flux across the channel quoted in Table 1 was calculated using eq 1,[50,52] (rates k defined as in Table 1) with an assumed extracellular concentration (c_{cis}) of 10 μM (approximately a clinically relevant concentration[53,54]), with no antibiotic present in the periplasmic space ($c_{trans} = 0$).

$$J = \frac{k_{on}^{cis} \cdot c_{cis}}{k_{off}^{total} + (k_{on}^{cis} \cdot c_{cis})} \cdot \frac{k_{on}^{trans} \cdot k_{off}^{total}}{k_{on}^{cis} + k_{on}^{trans}} \quad (1)$$

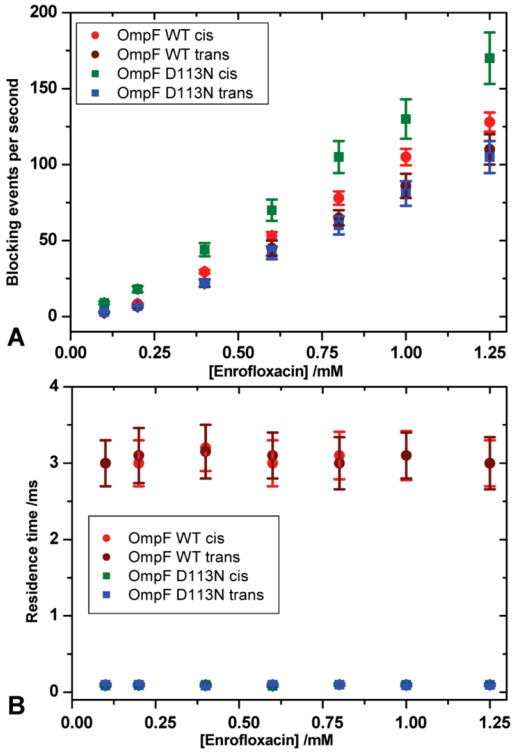

Figure 3. Kinetic analysis of current blocking events by enrofloxacin, per monomer of OmpF (conditions as in Figure 2): (A) the number of binding events per second per monomer, ν, is linear with enrofloxacin concentration and strongly dependent on the side of addition in case of D113N; (B) the dwell time τ is independent of the side of addition; the points in the case of D113N overlap.

TABLE 1: Association and Dissociation Constants Obtained by Single-Channel Conductance Measurements on OmpF[a]

enrofloxacin	k_{on}^{cis} 1/(s•M)	k_{on}^{trans} 1/(s•M)	k_{off}^{total} 1/s	K_{eq} 1/M	$J_{cis\rightarrow trans}$ 1/s
WT OmpF					
−50 mV	17000	15000	333	96	0.08
50 mV	5000	4167	700	13	0.02
D113N OmpF					
−50 mV	31000	14000	11000	4	0.10
50 mV	8000	6500	11000	1.3	0.04

[a] k_{on}^{cis} and k_{on}^{trans} correspond to the association rate from the cis or trans side, respectively (with the possibility of different activation barriers), while k_{off}^{total} is the sum dissociation rate towards either side (the separate directions not being measurable independently). K_{eq} is the resulting total equilibrium constant, and $J_{cis\rightarrow trans}$ is the trans-membrane flux from the cis to trans side, both assuming a single affinity site.[50]

As can be seen in Table 1, the flux under this assumption is very similar for the WT and mutant porin. In both cases, it is higher at negative trans-membrane voltages corresponding to the biological potential across the outer membrane.[55] The model used to calculate the flux relies on counting the molecules passing in and out of the pore on each side, using the on- and off-rates calculated, assuming that translocation occurs through at least one measured site located inside the channel.[50] We observe that the on-rate is first-order with bulk antibiotic concentration, and that the probability density function of the intrachannel dwell time fits perfectly to a single exponential decay (see Supporting Information Figure S1) and is invariant with the side of addition (Figure 3). In such cases, it is generally assumed that the measured rates in fact correspond to a single affinity site inside the channel.[56,57]

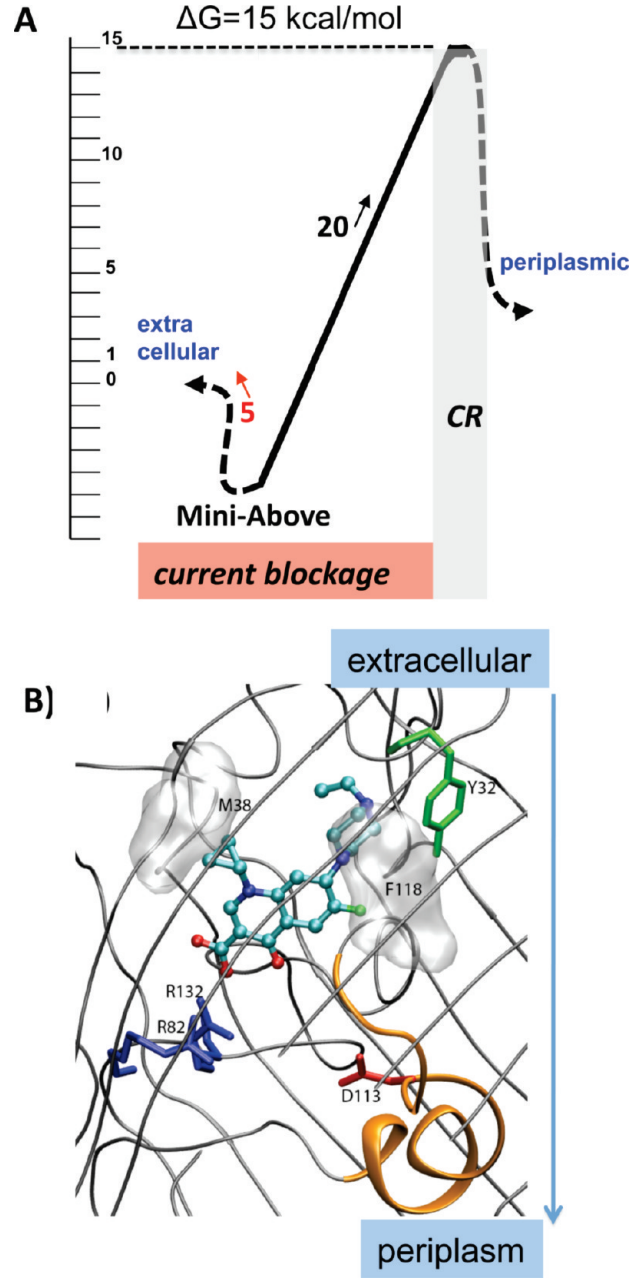

Figure 4. (A) 1D free energy profile for cis side addition of enrofloxacin to WT OmpF, with the affinity site at the channel mouth. The gray shading highlights the location of the CR, while the red color labels the region where the pore is occluded. (B) Molecular detail of the preferred minimum, above the CR, Mini-Above, showing the interacting residues of OmpF (colored by residue types, the ones involved in Hb's are displayed as sticks and those involved in Hc's are displayed by molecular surface) with enrofloxacin (colored by atom names) (see Figure 1 for coloring code).

We use MD simulations to further investigate the unusually strong binding in the case of the WT porin and rationalize the drastic change in kinetics after mutation.

MD Simulations. We performed accelerated MD[41] simulations of the translocation of enrofloxacin through WT OmpF and characterized the free energy minima visited along the process. Calculations of the free energy barriers connecting each minimum allowed us to reconstruct the complete 1D free energy profile corresponding to the translocation of enrofloxacin. The profile reveal a high main effective barrier (ΔG) of 15 kcal/mol, defined as the difference in energy between the highest barrier and the entrance of the channel (Figure 4A). Unexpect-

TABLE 2: Calculated Minimum Cross Section Areas and Energy Transfer Probabilities to the Two Tryptophans, Associated with the Preferential Energy Minima of Enrofloxacin (Enro) in WT and D113N OmpF[a]

	area (Å^2)			energy transfer probability (%)	
system	OmpF total	OmpF+Enro total	OmpF+Enro ion accessible	W214	W61
WT	22 ± 4	22 ± 4	5 ± 4	88 ± 8	75 ± 9
D113N	21 ± 4	41 ± 5	4 ± 5	94 ± 1	19 ± 17

[a] The area calculations compare the solvent-accessible internal area obtained from (i) independent simulations of the unbound, free form of OmpF (1st column); (ii) simulations of the complexes "OmpF+Enro" with enrofloxacin in its preferential minimum (in the second column enrofloxacin was manually removed prior to the accessibility calculation to obtain a total internal area, while in the third column enrofloxacin is left in to obtain the ion accessible area). The energy transfer calculations show that when enrofloxacin is bound in the preferential minimum, the energy transfer probability from the two tryptophans is very different for WT and D113N.

edly, we find an absence of minima at the CR, instead the deepest energy minimum to be located well above the CR (Mini-Above in Figure 4A). We subsequently performed an equilibrium MD simulation to elucidate the structural and dynamical properties at Mini-Above. In this minimum, enrofloxacin is in a strong affinity site defined by durable interactions with several residues in OmpF; it forms Hb's with residues R132, R82 and Y32, while it anchors in hydrophobic pockets at residues M38 and F118 (Figure 4B). The stability of enrofloxacin in Mini-Above is confirmed by the low calculated rmsf's showing a very low flexibility of the antibiotic atoms: an average of ~0.36 Å. As a comparison, the rmsf of ampicillin was found to be 2.5 times higher in the same region.[58] As enrofloxacin adopts a close to horizontal orientation in Mini-Above, perpendicular to the *Z*-axis of diffusion, we expect the channel to be occluded to ionic conductance. This is confirmed by the calculated surface accessible area as cross sections along the channel, which shows that, when enrofloxacin is bound in Mini-Above, it leaves as little as 5 Å^2 of space available to ions (Table 2). The calculated accessible area along each step of the metadynamics simulation also shows that the antibiotic can repeatedly occlude the pore even before entering the CR and effectively translocate (see Supporting Information Figure S2).

With sufficient biased simulation time, enrofloxacin moves away from its localization at Mini-Above and can overcome the high energy barrier to traverse the CR. In the process, enrofloxacin adopts a vertical orientation, parallel to the axis of diffusion with its carboxyl group pointing down, allowing the antibiotic to quickly slide down and exit the channel on the periplasmic side. Along this path, we note the Hb's between the antibiotic oxygen atoms (Figure 1B) and the cluster of basic residues opposite the L3 loop (Figure 1A).

We then set to study the passage of enrofloxacin through the OmpF mutant D113N, and find that the translocation path of enrofloxacin is very different from that of WT OmpF (Figure 5A). In particular, in the case of the D113N mutant, the deepest energy minimum found by enrofloxacin is located at the CR (Mini-CR). The effective energy barrier to translocate in now much lower, $\Delta G = 11$ kcal/mol, compared to that calculated for WT OmpF. In fact, the translocation of enrofloxacin happens in a much shorter biased simulation time in the case of D113N (26 ns) compared to the WT (36 ns). In-depth analysis of the molecular details reveals that, in the case of the D113N mutant, unlike for WT OmpF, we do not observe any durable specific interactions when enrofloxacin is above the CR. Upon mutation, the CR becomes more hydrophobic, which allows a preferential accommodation of enrofloxacin. The antibiotic crosses the CR and further translocates not with its polar carboxyl but rather with its hydrophobic group pointing down. As seen in Figure 5B, in Mini-CR, when enrofloxacin is bound at the CR, it makes stable Hb's with S125 and many Hc's (with F118, L115, P116).

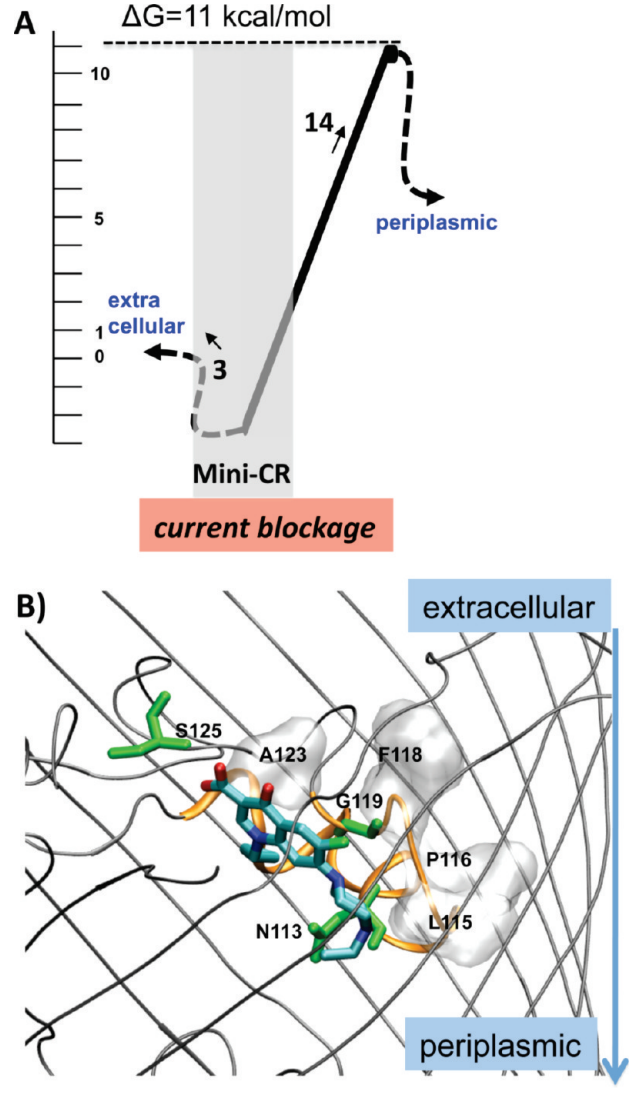

Figure 5. (A) 1D free energy profile of cis side addition of enrofloxacin to D113N OmpF with the affinity site in the CR. (B) Molecular details of enrofloxacin in the preferential minimum at CR, Mini-CR (see Figure 4 for legend).

There, the accessible area calculations reveal total occlusion of the pore when enrofloxacin is in Mini-CR (see Figure 5A), its preferential affinity site at the CR (Table 2).

Our simulation revealing a favorable binding site at the cis channel mouth in the case of WT OmpF, with easy access from the cis direction, does not explain the conductance measurements, where we found that on-rates of enrofloxacin are nearly independent of the side of addition ($k_{on}^{cis} \approx k_{on}^{trans}$). To investigate this apparent contradiction, we performed an additional meta-

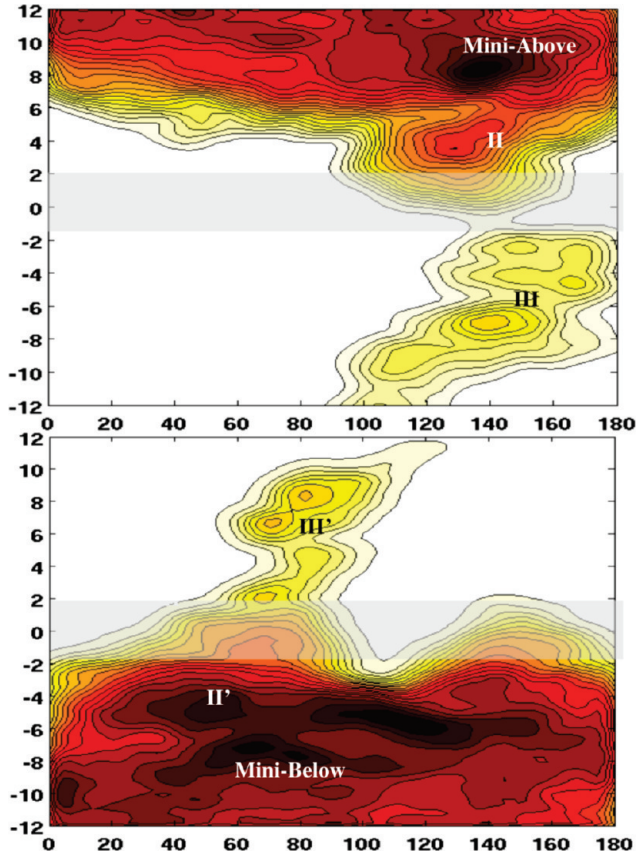

Figure 6. Complete FES for enrofloxacin translocating thorugh WT OmpF, associated with the reaction pathway along the subspace of the two variables, the distance Z along Y (Z = 0 corresponds to the center of the constriction region) and the angle θ along X (see methods). Each isoline corresponds to a different color gradient and to 1 kcal/mol. (A) Simulation starting with cis (extracellular) side addition of enrofloxacin, and (B) simulation starting with trans (periplasmic) side addition.

dynamics simulation, starting with enrofloxacin in the periplasmic (trans) side of the WT OmpF. Interestingly, the process sampled is very similar to the "cis addition" in an inverse symmetric way (Figure 6). In particular we note (i) the absence of a deep energy minimum at the CR and instead its peripheral localization, in this case well below the constriction (Mini-Below), and (ii) the need to overcome a high energy barrier for enrofloxacin to translocate (from the periplasmic to the extracellular side). Furthermore, the area calculations show that in Mini-Below, enrofloxacin only leaves ~6 Å^2 of accessible area to ions. Our molecular analysis reveals that the total pore occlusion is here again explained by the horizontal orientation adopted by enrofloxacin in Mini-Below (Figure 7). This alternative affinity site below the CR is also defined by specific and well-defined interactions: Hb's with R270 and Q262, and Hc's with M114, P116, and L115 (Figure 7).

The complete processes (cis, trans) of translocations through the channels are schematized in Figure 8, which sums up the location of affinity sites and free energy profiles obtained. From these results, we propose that in the case of WT OmpF, there is a prohibitive energy barrier for enrofloxacin in the center of the channel, separating two binding sites on the two opposite ends of the channel. This symmetry explains the similar on- and off-rates measured on the two sides for WT OmpF. In this case, the number of translocation events would be low enough to be experimentally insignificant compared to the backflow of molecules. No measurable substrate traffic between the sites accounts for the exponential dwell-time distribution. The

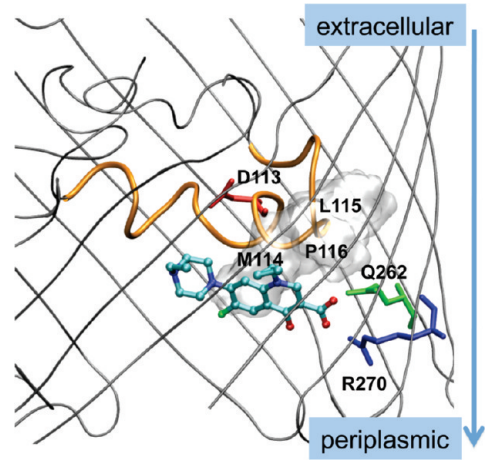

Figure 7. Molecular interaction of enrofloxacin with WT OmpF in the preferential affinity site of the trans addition simulation, below the CR. We highlight the specific interactions (Hb's and Hc's) between enrofloxacin and the residues of the channel wall (see legend in Figure 4).

residence time distribution would correspond to the same potential depth, but not to the same location of the affinity site.

The simulations suggest that, in the case of the WT OmpF, the pore occlusion to ionic conductance is due to two distinct, symmetric sites, while, in the case of D113N, it happens at one well-defined affinity site at the CR. Additional simulations of the "trans addition" of enrofloxacin also confirmed such central localization of the preferential affinity site in the case of D113N. We thus expect that, in the case of D113N, we calculated the flux with an applicable model, while in the case of WT OmpF, the calculated fluxes relying on a single site assumption (in Table 1) would be invalid.

This scenario has so far never been considered in theoretical analyses of affinity-enhanced translocation[52] or taken as a possibility in the interpretation of experimental results.[42] To be able to confidently propose this correction to the usually applied calculation of translocation kinetics, we aim to verify the differential localization of the affinity sites predicted by the simulations independently using spectroscopic techniques.

Fluorescence Studies. When a solution of enrofloxacin is added to OmpF-containing proteoliposomes, a quenching in the inherent tryptophan fluorescence is observed. This quenching shows antibiotic interaction involving at least one of the two distinct OmpF tryptophans (W61 and W214), potentially enabling us to confirm the location of the preferential affinity site. The antibiotic quenching data alone does not allow the discrimination of interactions with either fluorophore. We may, however, follow the modification of the tryptophans' individual quenching constants by site-specific quenchers in the presence of enrofloxacin,[24,59] thereby deducing the perturbation of the local environment. When quenching OmpF fluorescence with iodide or acrylamide, the Stern−Volmer plots display a downward curvature, showing a different accessibility of the two tryptophan residues to the quenchers. We find that W61 at the intersubunit region is more accessible to acrylamide, and W214 at the interface with phospholipid headgroups is more accessible to iodide. The quenching process is thus described by a modified Stern−Volmer equation (eq 2):[60]

$$F_0 - F = F_{0a}\frac{K_{SVa}|Q|}{1 + K_{SVa}|Q|} \qquad (2)$$

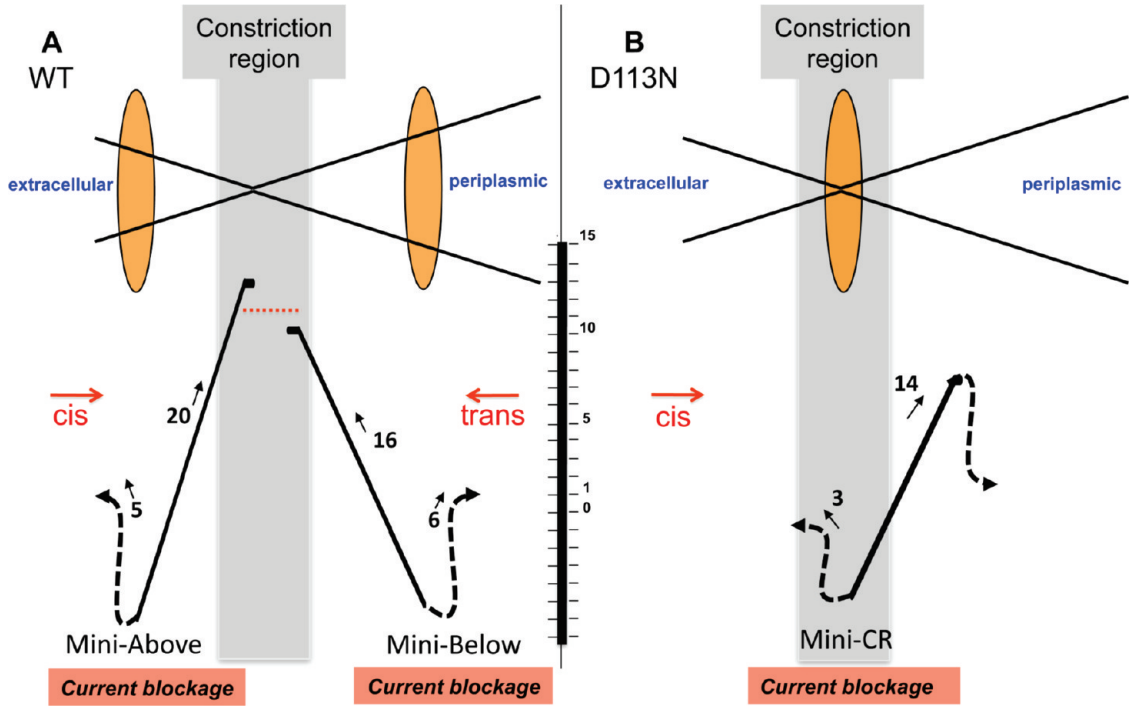

Figure 8. Scheme of the complete translocation process highlighting the localization of affinity sites in the WT and D113N OmpF, as in Figure 4. (A) In the case of WT OmpF, there are two affinity sites corresponding to ion current blockages symmetrically placed at the two ends of the channel, while (B) in the case of D113N OmpF there is only one affinity site, at the CR.

TABLE 3: Stern−Volmer Constants (K_a) and Accessible Fractions (f_a) of the Fluorescence Quenching of the OmpF Tryptophans by Acrylamide and Iodide, with and without the Addition of 7.4 μM Enrofloxacin

	no drug		enrofloxacin	
WT	K_a (M s^{-1})	f_a	K_a (M s^{-1})	f_a
acrylamide	3.8(±0.2)	0.6(±0.2)	1.9(±0.3)	0.7(±0.1)
I^-	2.8(±0.4)	0.4(±0.2)	0.4(±0.1)	0.7(±0.1)
	no drug		enrofloxacin	
D113N	K_a (M s^{-1})	f_a	K_a (M s^{-1})	f_a
acrylamide	2.4(±0.1)	0.8(±0.2)	1.7(±0.3)	0.7(±0.1)
I^-	2.7(±0.5)	0.2(±0.2)	11.7(±1.9)	0.2(±0.1)

where F_{0a} is the fluorescence intensity of the quencher-accessible fraction in the absence of quencher, and F is the fluorescence intensity in the presence of quencher; K_{SVa} is the Stern−Volmer quenching constant of the accessible fraction and $[Q]$ is the concentration of quencher. The accessible fraction (f_a) can be measured at saturation by taking the ratio of F_{0a}/F_0.

We find that upon enrofloxacin addition, the measured quenching is perturbed, and the changes in K_{SVA} values for the two quenchers in the presence of enrofloxacin are very different between WT OmpF and D113N OmpF (Table 3). In the case of the WT OmpF, addition of enrofloxacin results in a significant decrease of K_{SVa} for both iodide and acrylamide, which suggest the preferential localization of enrofloxacin at a site near both tryptophans. For the mutant D113N, only the acrylamide Stern−Volmer constant is strongly reduced by enrofloxacin, suggesting the preferential interaction of the antibiotic with W61 in the interior of the channel. In addition, the Stern−Volmer constant for iodide is increased, indicating greater exposure of the external W214 to surrounding iodide.

To be able to rationalize the tryptophan interaction specificity obtained by fluorescence as a precise intrachannel location and compare it to the model proposed by computer simulations, we calculated the energy transfer efficiency between the two tryptophans and the enrofloxacin. As done previously for moxifloxacin and WT OmpF,[24] the calculation was performed based on the angles and distances (provided by the equilibrium simulation of each preferential minimum), and the overlap integral from spectroscopy (see Supporting Information Figure S3). We report in Table 2 the resulting energy transfer efficiencies for WT and D113N, along the equilibrium simulation of Mini-Above for WT OmpF and of Mini-CR for D113N OmpF. We observe that, in Mini-Above, there is strong energy transfer from both tryptophans with no clear distinction, due to the near-horizontal conformation of enrofloxacin between the two tryptophan residues W61 and W214. For D113N, however, the energy transfer efficiency calculated in Mini-CR shows a clear preference for W61 (Table 2). These calculations agree remarkably well with the acrylamide and iodide quenching measurements obtained from fluorescence studies (Table 3).

The measured greater exposure of W214 to the surrounding solution in the case of D113N could be explained by a conformational change of the channel during translocation of enrofloxacin. Indeed, in the course of the standard MD simulation at the preferential affinity site (Mini-CR), we note a significant expansion of the D113N porin channel barrel at the CR. The minimal cross section area (averaged over the standard MD simulation of Mini-CR) increases to a value of 41 Å^2 compared to the value of 21 Å^2 for the reference simulation of D113N OmpF without the antibiotic. Such an expansion of the channel only happens in the case of D113N and is probably due to the steric strain of the enrofloxacin in the constriction (Table 2), confirming the possibility of a conformational change.

Conclusion

Ion current fluctuation analysis revealed an exceptionally long residence time for enrofloxacin in the WT OmpF channel. Supported by the MD simulations, we propose that enrofloxacin has two distinct affinity sites in which it blocks the ionic current

in WT OmpF, one at the extracellular and one at the periplasmic end of the protein channel (Figure 8). These symmetric peripheral affinity sites are indistinguishable by conductance measurements as they are separated by a large energy barrier, which inhibits the flux. A symmetric double binding site scenario has so far not been observed and is usually not considered in affinity-facilitated permeation.[61] Using complementary techniques, we were able to recognize this phenomenon and show that, in the case of WT OmpF, the common analytical method[50,52] gives a probable significant overestimate of the actual trans-membrane flux.

We also demonstrated the drastic effect on channel permeation by the single amino acid substitution D113N decreasing the equilibrium constant more than an order of magnitude. Replacing the negative by a neutral residue in the channel constriction results in a much lower main effective barrier for the translocation of enrofloxacin.

The shift in affinity site from peripheral to central, resulting in a lower translocation barrier, gives important new insight into affinity-enhanced translocation. We show that, for influx screening, it is not sufficient to confirm high affinity, in analogy to specific channels.

This example demonstrates how translocation through a nanoscopic channel depends not only on the strength of the substrate-channel interaction, but also on a local affinity site counteracting the conformational entropy change at the smallest constriction.

Acknowledgment. The authors are grateful for financial support through the EU Grant MRTN-CT-2005-019335 (translocation) and from Jacobs University Bremen. We thank Peter Eaton and Paolo Ruggerone for scientific discussions. We thank also the following centers for providing CPU time: CASPUR (Roma), CINECA (Bologna), and COSMOLAB (Cagliari).

Supporting Information Available: Dwell time histogram of enrofloxacin channel blockages in WT and D113N OmpF. Ion-accessible area through the entire simulation path of enrofloxacin translocation in WT and D113N OmpF. Overlap of OmpF emission and enrofloxacin absorption spectra. This material is available free of charge via the Internet at http://pubs.acs.org.

References and Notes

(1) Yoshimura, F.; Nikaido, H. *Antimicrob. Agents Chemother.* **1985**, *27*, 84–92.
(2) Nikaido, H. *Science* **1994**, *264*, 382–388.
(3) Mortimer, P. G.; Piddock, L. J. *J. Antimicrob. Chemother.* **1993**, *32*, 195–213.
(4) Cowan, S. W.; Schirmer, T.; Rummel, G.; Steiert, M.; Ghosh, R.; Pauptit, R. A.; Jansonius, J. N.; Rosenbusch, J. P. *Nature* **1992**, *358*, 727–733.
(5) Benz, R.; Schmid, A.; Nakae, T.; Vos-Scheperkeuter, G. H. *J. Bacteriol.* **1986**, *165*, 978–986.
(6) Nestorovich, E. M.; Danelon, C.; Winterhalter, M.; Bezrukov, S. M. *Proc. Natl. Acad. Sci. U.S.A.* **2002**, *99*, 9789–9794.
(7) Kresse, H.; Belsey, M. J.; Rovini, H. *Nat. Rev. Drug. Discovery* **2007**, *6*, 19–20.
(8) Andriole, V. T. *Clin. Infect. Dis.* **2005**, *41*, S113−S119.
(9) Chenia, H. Y.; Pillay, B.; Pillay, D. *J. Antimicrob. Chemother.* **2006**, *58*, 1274–1278.
(10) Hooper, D. C. *Drug Resist. Updates* **1999**, *2*, 38–55.
(11) Delcour, A. H. *Biochim. Biophys. Acta* **2009**, *1794*, 808–816.
(12) Higgins, P. G.; Fluit, A. C.; Schmitz, F. J. *Curr. Drug Targets* **2003**, *40*, 181–190.
(13) Chevalier, J.; Mallea, M.; Pages, J. M. *Biochem. J.* **2000**, *348*, 223–227.
(14) Berlanga, M.; Ruiz, N.; Hernandez-Borrell, J.; Montero, T.; Vinas, M. *Can. J. Microbiol.* **2000**, *46*, 716–722.
(15) De, E.; Basle, A.; Jaquinod, M.; Saint, N.; Mallea, M.; Molle, G.; Pages, J. M. *Mol. Microbiol.* **2001**, *41*, 189–198.
(16) Begic, S.; Worobec, E. A. *Can. J. Microbiol.* **2007**, *53*, 710–719.
(17) James, C. E.; Mahendran, K. R.; Molitor, A.; Bolla, J. M.; Bessonov, A. N.; Winterhalter, M.; Pages, J. M. *PLoS One* **2009**, *4*, e5453.
(18) Pages, J. M. *Med. Sci. (Paris)* **2004**, *20*, 346–351.
(19) Vidal, S.; Bredin, J.; Pages, J. M.; Barbe, J. *J. Med. Chem.* **2005**, *48*, 1395–1400.
(20) Bezrukov, S. M.; Kullman, L.; Winterhalter, M. *FEBS Lett.* **2000**, *476*, 224–228.
(21) Lizondo, M.; Pons, M.; Gallardo, M.; Estelrich, J. *J. Pharm. Biomed. Anal.* **1997**, *15*, 1845–1849.
(22) Sun, J.; Sakai, S.; Tauchi, Y.; Deguchi, Y.; Chen, J.; Zhang, R.; Morimoto, K. *Eur. J. Pharm. Biopharm.* **2002**, *54*, 51–58.
(23) Neves, P.; Berkane, E.; Gameiro, P.; Winterhalter, M.; de Castro, B. *Biophys. Chem.* **2005**, *113*, 123–128.
(24) Mach, T.; Neves, P.; Spiga, E.; Weingart, H.; Winterhalter, M.; Ruggerone, P.; Ceccarelli, M.; Gameiro, P. *J. Am. Chem. Soc.* **2008**, *130*, 13301–13309.
(25) Prilipov, A.; Phale, P. S.; Van Gelder, P.; Rosenbusch, J. P.; Koebnik, R. *FEMS Microbiol. Lett.* **1998**, *163*, 65–72.
(26) Garavito, R. M.; Rosenbusch, J. P. *Methods Enzymol.* **1986**, *125*, 309–328.
(27) Montal, M.; Mueller, P. *Proc. Natl. Acad. Sci. U.S.A.* **1972**, *69*, 3561–3566.
(28) Hoenger, A.; Pages, J. M.; Fourel, D.; Engel, A. *J. Mol. Biol.* **1993**, *233*, 400–413.
(29) Danelon, C.; Brando, T.; Winterhalter, M. *J. Biol. Chem.* **2003**, *278*, 35542–35551.
(30) Wiechelman, K. J.; Braun, R. D.; Fitzpatrick, J. D. *Anal. Biochem.* **1988**, *175*, 231–237.
(31) Smith, P. K.; Krohn, R. I.; Hermanson, G. T.; Mallia, A. K.; Gartner, F. H.; Provenzano, M. D.; Fujimoto, E. K.; Goeke, N. M.; Olson, B. J.; Klenk, D. C. *Anal. Biochem.* **1985**, *150*, 76–85.
(32) Plancon, L.; Chami, M.; Letellier, L. *J. Biol. Chem.* **1997**, *272*, 16868–16872.
(33) Paternostre, M. T.; Roux, M.; Rigaud, J. L. *Biochemistry* **1988**, *27*, 2668–2677.
(34) Knol, J.; Sjollema, K.; Poolman, B. *Biochemistry* **1998**, *37*, 16410–16415.
(35) Ceccarelli, M.; Danelon, C.; Laio, A.; Parrinello, M. *Biophys. J.* **2004**, *87*, 58–64.
(36) Procacci, P.; Darden, T. A.; Paci, E.; Marchi, M. *J. Comput. Chem.* **1997**, *18*, 1848–1862.
(37) Im, W.; Roux, B. *J. Mol. Biol.* **2002**, *319*, 1177–1197.
(38) Cornell, W. D.; Cieplak, P.; Bayly, C. I.; Gould, I. R.; Merz, K. M.; Ferguson, D. M.; Spellmeyer, D. C.; Fox, T.; Caldwell, J. W.; Kollman, P. A. *J. Am. Chem. Soc.* **1995**, *117*, 5179–5197.
(39) Robertson, K. M.; Tieleman, D. P. *FEBS Lett.* **2002**, *528*, 53–57.
(40) Rostovtseva, T K.; Nestorovich, E. M.; Bezrukov, S. M. *Biophys. J.* **2002**, *82*, 160–169.
(41) Laio, A.; Parrinello, M. *Proc. Natl. Acad. Sci. U.S.A.* **2002**, *99*, 12562–12566.
(42) Danelon, C.; Nestorovich, E. M.; Winterhalter, M.; Ceccarelli, M.; Bezrukov, S. M. *Biophys. J.* **2006**, *90*, 1617–1627.
(43) Laio, A.; Rodriguez-Fortea, A.; Gervasio, F. L.; Ceccarelli, M.; Parrinello, M. *J. Phys. Chem. B* **2005**, *109*, 6714–6721.
(44) Kullman, L.; Winterhalter, M.; Bezrukov, S. M. *Biophys. J.* **2002**, *82*, 803–812.
(45) Colquhoun, D.; Sigworth, F. J. Fitting and statistical analysis of single channel records. In *Single-Channel Recording*; Sakmann, B., Neher, E., Eds.; Plenum Press: New York, 1995; pp 483−587.
(46) Colquhoun, D.; Hawkes, A. G. *Philos. Trans. R. Soc. London B: Biol. Sci.* **1982**, *300*, 1–59.
(47) Horn, R.; Lange, K. *Biophys. J.* **1983**, *43*, 207–223.
(48) Hall, P. *J. Appl. Probab.* **1983**, *20*, 585–599.
(49) Beard, D. A.; Qian, H. *Chemical Biophysics: Quantitative Analysis of Cellular Systems*; Cambridge University Press: Cambridge, UK, 2008; Chapter 5.
(50) Schwarz, G.; Danelon, C.; Winterhalter, M. *Biophys. J.* **2003**, *84*, 2990–2998.
(51) Sen, K.; Hellman, J.; Nikaido, H. *J. Biol. Chem.* **1988**, *263*, 1182–1187.
(52) Bezrukov, S. M.; Berezhkovskii, A. M.; Szabo, A. *J. Chem. Phys.* **2007**, *127*, 115101.
(53) Nielsen, P.; Gyrd-Hansen, N. *Pharmacol. Toxicol.* **1997**, *80*, 246–250.
(54) Vance-Bryan, K.; Guay, D. R.; Rotschafer, J. C. *Clin. Pharmacokinet.* **1990**, *19*, 434–461.
(55) Stock, J. B.; Rauch, B.; Roseman, S. *J. Biol. Chem.* **1977**, *252*, 7850–7861.
(56) Berezhkovskii, A. M.; Bezrukov, S. M. *J. Phys.: Condens. Matter* **2007**, *19*, 065148.

(57) Bernasconi, C. F.; Weisberger, A. *Investigation of Rates and Mechanisms of Reactions, Part 1: General Considerations and Reactions at Conventional Rates*; Wiley-Interscience: New York, 1986.

(58) Hajjar, E.; Mahendran, K. R.; Kumar, A.; Bessonov, A. Petrescu, M.; Weingart, H.; Ruggerone, P.; Winterhalter, M.; Ceccarelli, M. *Biophys. J.* **2010**, *98*, 569−575.

(59) Neves, P.; Sousa, I.; Winterhalter, M.; Gameiro, P. *J. Membr. Biol.* **2009**, *227*, 133–140.

(60) Lakowicz, J. R. *Principles of Fluorescence Spectroscopy*; Springer Verlag: Heidelberg, Germany, 2006; Chapters 4, 10, 11.

(61) Berezhkovskii, A. M.; Pustovoit, M. A.; Bezrukov, S. M. *J. Chem. Phys.* **2002**, *116*, 9952–9956.

JP911485K